ATOMIC FORCE MICROSCOPY FOR UNIVERSITY STUDENTS APPLICATIONS IN BIOMATERIALS

S.V. Kontomaris[1*], A. Stylianou[1,2*]

[1]Biomedical Optics and Applied Biophysics Laboratory, School of Electrical and Computer Engineering,

National Technical University of Athens,

[2]Cancer Biophysics Laboratory, Department of Mechanical and Manufacturing Engineering, Faculty of Engineering, University of Cyprus, Cyprus

*Corresponding Authors: stkontomaris@gmail.com / stylianou.c.andreas.1@ucy.ac.cy

Abstract

Atomic Force Microscopy (AFM) is a powerful tool regarding the investigation of the structural and the mechanical properties of a wide range of materials including biomaterials. It provides the ability to acquire high resolution images of biomaterials in nanoscale. In addition, it provides information about the response of specific areas under controlled applied force which leads to the mechanical characterization of the sample in nanoscale. The broad band of information provided by AFM have been established it as a complete scientific instrument with tremendous impact in modern research activity. In this paper, a general overview of the basic operation and functions of AFM is presented for applications in biomaterials. The basic operation is explained in detail with focus on the real interactions which are taking place in nanoscale during imaging. Furthermore, its ability to provide the mechanical characterization (force curves) of specific areas in nanoscale is presented. The basic models of applied mechanics which are used for the processing of the data obtained by force curves are presented. In conclusion, a general overview of the Atomic Force Microscopy for biophysics applications is provided which will contribute to the complete presentation of the instrument for university students and young researchers.

Keywords: Atomic Force Microscopy (AFM), Biophysics, Nanoscale Imaging, Force Spectroscopy, Applied Mechanics in Nanoscale

1. Introduction

Atomic Force Microscopy (AFM) belongs to the scanning probe microscopes family [1] which rely their operation on the interactions of a small tip which is based on the edge of a sensitive cantilever with a sample's surface in nanoscale. The purpose for the development of the AFM was the imaging of non – conducting samples [2]. Firstly, the basic goal was to improve the imaging resolution analysis comparing to the optical microscopy. However, AFM was proved as a powerful instrument which was able to provide a wide range of information apart from imaging. In particular, the force spectroscopy measurements combined with the high resolution imaging techniques provide the ability for the complete characterization of a sample's surface in nanoscale. In addition, AFM has a major advantage comparing to other microscopy techniques (i.e. Scanning and Transmission Electron Microscopy- SEM, TEM) which is the ability for the acquisition of high resolution images of native biological samples

in environmental or liquid conditions (i.e. avoiding sample preparation which in many cases is responsible for artifacts) [2].
Nowadays, there is a wide range of AFM applications, from imaging of the smallest biomolecules to the mechanical characterization of materials and biomaterials [2-14]. In this paper, the basic operation of AFM for imaging and mechanical measurements regarding biological samples is presented. The aim of this paper is to provide a broad band of information about the physical principles related to the AFM operation regarding university students and young scientists in the fields of Biophysics and Nanotechnology. Firstly, the basic parts of an AFM apparatus are presented. The imaging modes are explained in detail with focus on the physical principles of interactions that occur in nanoscale during the imaging procedure. Moreover, AFM images from real AFM experiments are presented. In addition, the ability of the AFM for the mechanical characterization in nanoscale is presented (force spectroscopy) and the basic contact mechanics models for the analysis of the AFM data are clearly mentioned. Furthermore, typical force curves obtained on biological samples are shown. The wide range of information about AFM measurements, regarding Biophysics, which is provided in this paper will contribute to the literature for university students and young scientists who want to verse on AFM basic theory and techniques.

2.1. Basic Operation

The basic operating principle of AFM is based on a sharp tip which is mounted on the edge of a flexible cantilever in order to scan a sample's surface [3, 16]. The tip comes in contact with the sample and "grazes" the sample, like the old fashion record-player needles in gramophones. The tip – samples' surface relative motion is performed using a piezoelectric actuator with sub – Angstrom accuracy. During the scanning procedure, the cantilever deflects and this motion which is based on the tip-samples' interaction is monitored by a laser beam pointing on the back of the cantilever (Figure 1). The laser beam is reflected towards to a photodetector in order to be recorded the cantilever's motion towards and away from the sample's surface during scanning. In addition, a feedback circuit which is connected to the cantilever deflection sensor is responsible to remain the tip –sample's surface interaction at a constant level by controlling the tip – sample's surface relative distance [15]. The feedback signal amount at each scanning point is being measured in order to construct a 3D image which represents the sample's surface topography. Consequently, the AFM systems generate images by "feeling" the surface, rather than "looking" at samples as the rest microscopes (e.g., optical microscope, scanning electron microscope) [17]. You may imagine the AFM as a blind man who use his finger or stick to feel a surface, but his world is at the nanometer scale [18].

2.2. Force vs distance

During the relative motion of tip – sample's surface, interaction forces arise. At large distances the resultant force is attractive (Van der Waals forces) [19]. On the contrary at small distances the resultant force is repulsive (overlapping of electron orbitals between tip – sample) [19]. These forces can be approximated using Lennard – Jones potential (Figure 2) [20]:

$$V(d) = 4\varepsilon\left[\left(\frac{d_m}{d}\right)^{12} - \left(\frac{d_m}{d}\right)^{6}\right] \quad (1)$$

Where, V, d is the intermolecular potential and the distance respectively between the two atoms or molecules, ε is the well depth (a measure of how strongly the two particles attract each other), d_m is the distance in which $V = 0$.

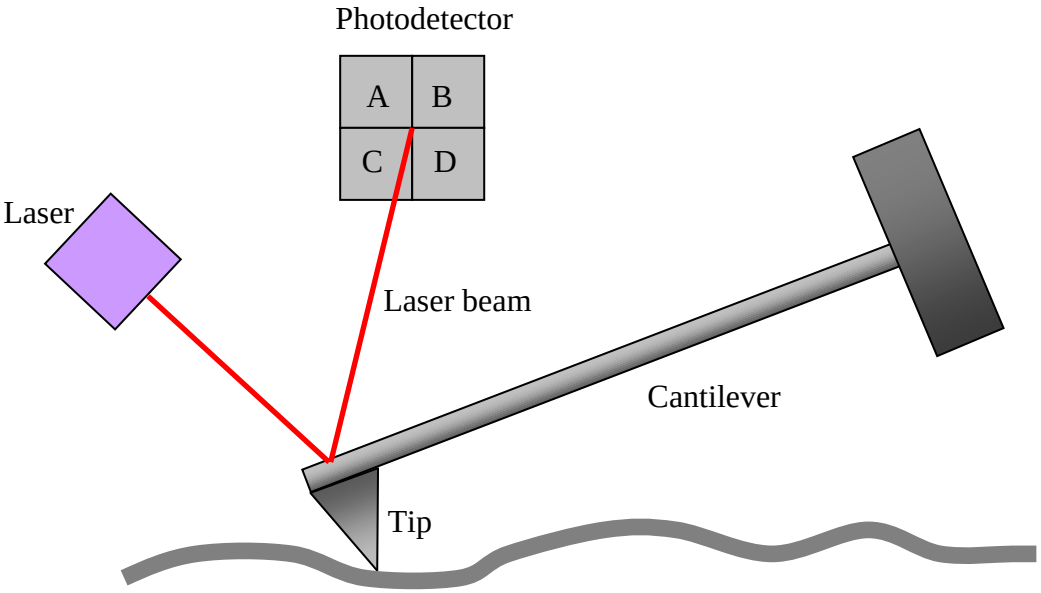

Figure 1: The basic operation of Atomic Force Microscopy. A sample's surface is being scanned by a tip which is mounted at the edge of a cantilever. The deflection of the cantilever is being monitored using a laser beam.

When the separation distance takes the value $d = d_{eq}$ (where, d_{eq} is the equilibrium distance) the total force is zero (Figure 3).
The forces which are applied between the tip and the sample's surface are presented in Figure 3. When $d > d_{eq}$ the resultant force is attractive and when $d < d_{eq}$ the resultant force is repulsive. The diagram in Figure 3a approximates the interaction forces between tip and the sample's surface. In Figure 3b the forces applied on the AFM tip in different regions are presented.

If , $d > d_{eq}$, $F_T = F_R - F_A < 0$
If , $d = d_{eq}$, $F_T = F_R - F_A = 0$
If, $d < d_{eq}$, $F_T = F_R - F_A > 0$

Where, F_R the repulsive force and F_A the attractive force and F_T the total force on the tip.

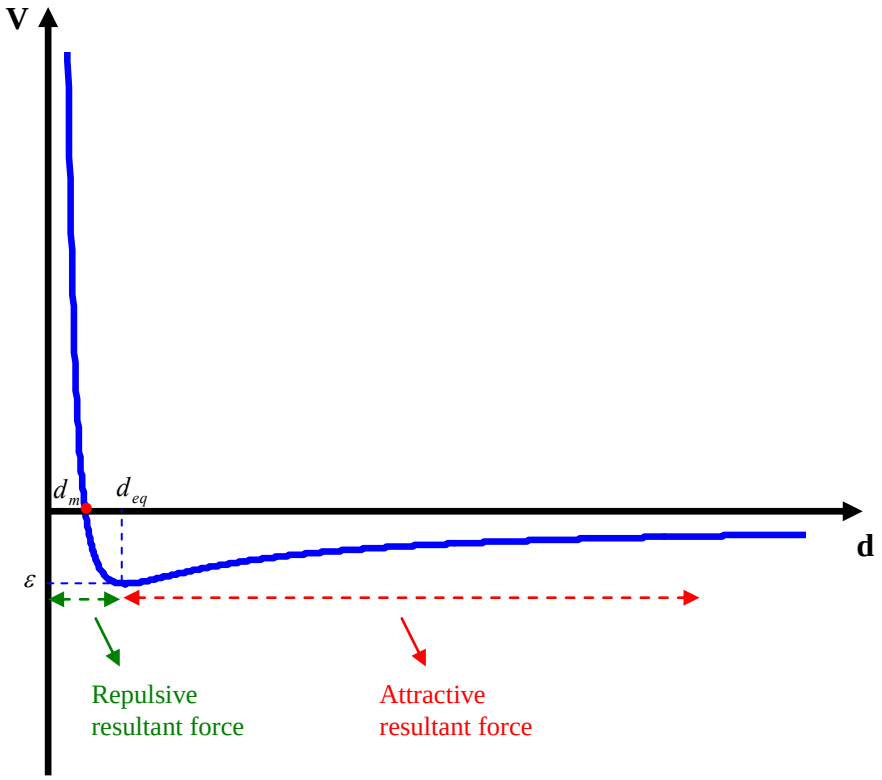

Figure 2: The Lennard – Jones potential. When $d > d_{eq}$ the resultant force is attractive and when $d < d_{eq}$ the resultant force is repulsive. When $d = d_{eq}$, the total force is zero, $\Sigma F = 0$.

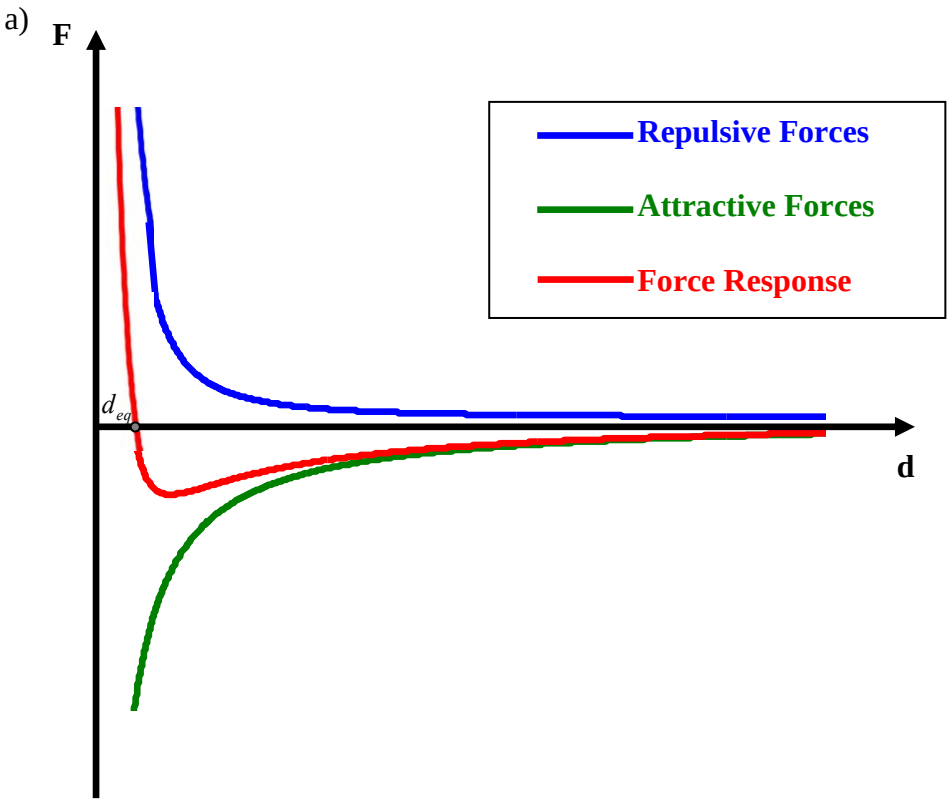

Figure 3a: Force – distance curves. Interaction forces versus distance between tip and sample's surface.

b)

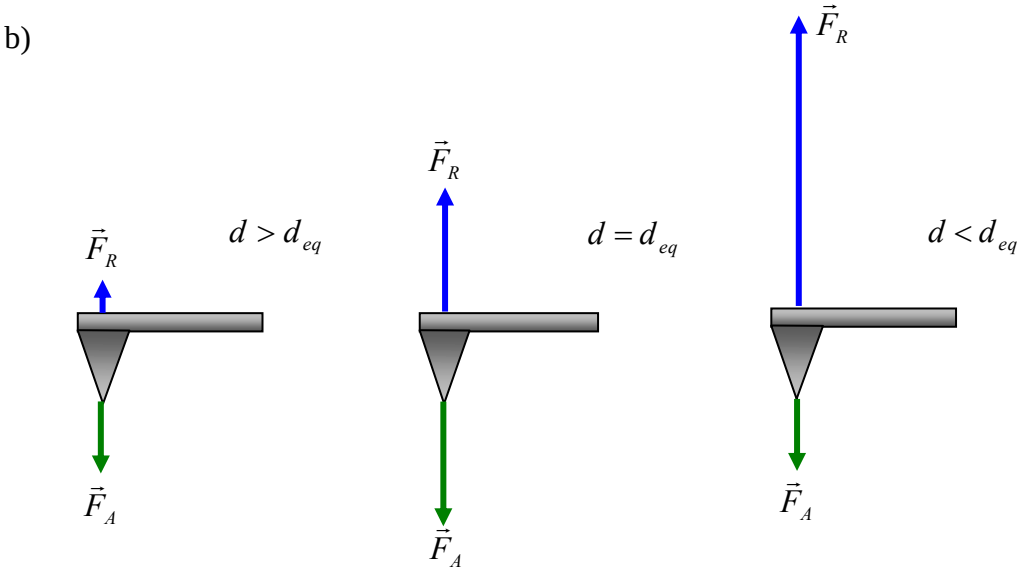

Figure 3b: Repulsive and attractive forces on the tip. Forces applied on the AFM tip in three different regions.

3. AFM imaging modes

Depending on the experiment and the sample that is being scanned, AFM can work in three basic imaging modes, the contact, the tapping and the non – contact mode. The force between the tip and the sample's surface defines the operation mode. Generally, the force between the AFM tip and the sample surface can be repulsive (if the tip – sample distance is less than 1nm) or attractive (if the tip – sample distance >100nm). Hence, in case that the force between the sample's surface and the tip is continuously repulsive, and the tip is always in contact with the sample, the operation mode is contact mode. On the contrary, if the force between tip – sample is continuously attractive, and the tip never touches the sample's surface, the operation mode is the non – contact mode. Furthermore, there is an additional mode, the intermittent mode or tapping mode in which cantilever is oscillated at a frequency near its resonance and the net force is attractive or repulsive depending on the tip's position.

3.1. Contact mode

The first imaging mode which was developed is the contact mode [21], in which the tip is always in contact with the sample's surface (Figure 4a). In contact mode, the cantilever's deflection remains constant (hence, the applied force on the sample's surface is always constant) during the scanning procedure. The resultant force on the sample is repulsive [22], despite the attractive forces on the tip due to the presence of a thin water layer on the sample. In order to minimize the attractive forces due to the water layer, the contact mode can be applied in aqueous environment.
Contact mode is the best choice for imaging flat and rigid surfaces. However, image artifacts are not always avoided (e.g. surface tilt) and dominate over the topography characteristics of the surface. The possibility of the domination of imaging artifacts increases when large areas (e.g. 100 μm x 100 μm) are being scanned or when imaging rate is too slow (e.g. 0.5 Hz). However, low – frequency scanning artifacts

could be avoided using the error mode, in which the cantilever's deflection signal is recorded in order to keep the response of the feedback fast [2, 23]. The error mode provides information about how well the desired applied force (i.e. the desired cantilever's deflection) is maintained during imaging. In contact mode the user can obtain height images, error or deflection images and lateral force images (see figure 4b). The deflection images are formed by the error signal, which is the difference, measured in volts by the photodetector, between the Setpoint and actual cantilever deflection. On the other hand, the Lateral force images (some manufactures call this kind of images as friction images) are formed by the cantilever's twisting motion when the tip passes over regions of varying friction. Contrast of lateral force images may have origin by changes in frictional properties across the sample or by variations in topography. Also, some manufactures may provide different kind of images like Zsensor images, which, briefly, use the movement of the optical lever detection assembly as monitored by a closed loop sensor to form images (see the third image in Figure 4b [24].

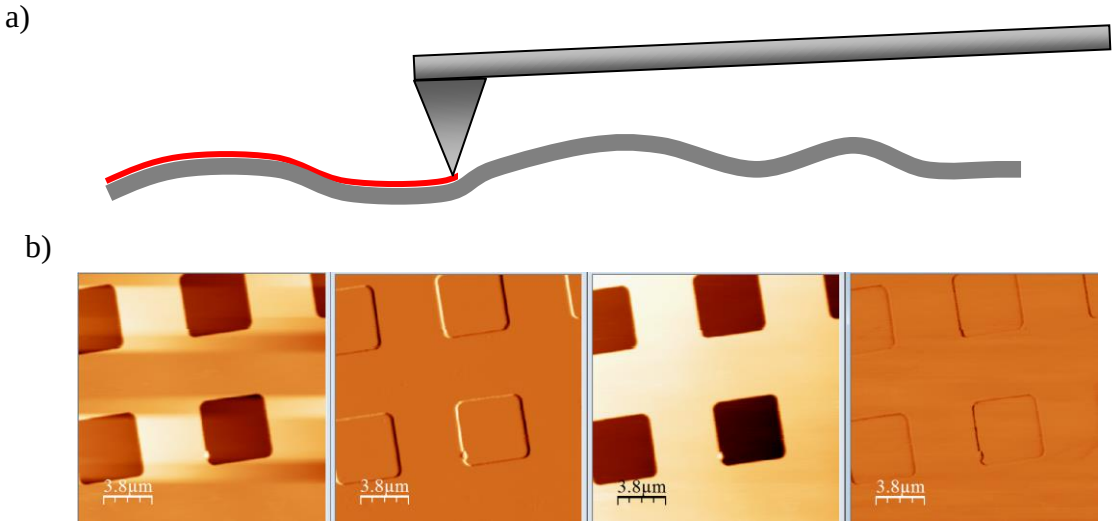

Figure 4: Contact mode imaging. a) In contact mode, the AFM tip is always in contact with the sample's surface. b) Images from contact mode. Height, Deflection, ZSensor and Lateral images, respectively of calibration grating (the images were taken with a Cypher ES, Asylum, Oxford Instruments microscope with PNP-TR, Nanoworld, v-shape probes).

3.2. Tapping mode

The aim of the tapping mode is to minimize the sample surface damages on soft compliant samples. Its operation is based on the monitoring of the oscillation amplitude. Firstly, the cantilever is oscillated near its resonance frequency with an initial value of amplitude which is damped when the tip touches the sample's surface. In addition, the resonance frequency, is modified by the tip-surface interaction (dominant repulsive interaction lead to an increase of the resonance frequency).
The recording of the feedback signal allows keeping a constant value to the tip's oscillation amplitude in order to obtain the topography of the sample. In tapping mode, the tip is not in continuously contact with the sample's surface (Figure 5), thus the possibility of damaging the sample is significantly reduced.

Tapping mode is the most appropriate mode for imaging soft biological samples with high resolution.

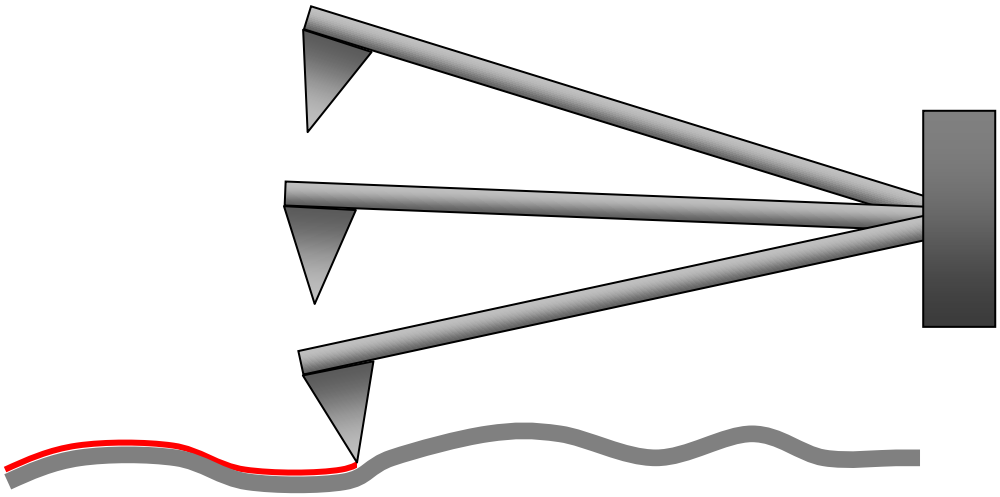

Figure 5: Tapping mode imaging. In tapping mode cantilever is oscillated with an initial value of amplitude which is damped when the tip touches the sample's surface. AFM tip hits repeatedly and slightly the sample's surface.

In the tapping mode, topography and phase images are simultaneously acquired so as to obtain information on different properties of the sample [17]. In Phase Imaging the detector signal is the phase φ, of the cantilever oscillations relative to the phase of drive signal [10]. AFM phase imaging goes beyond topographical features and it is the appropriate method for detecting variations in composition, friction and viscoelasticity enhancing contrast on heterogeneous samples [10,25].
In Figure 6, the exact same area of a collagen gel is presented, as it was imaged with contact and tapping mode respectively.

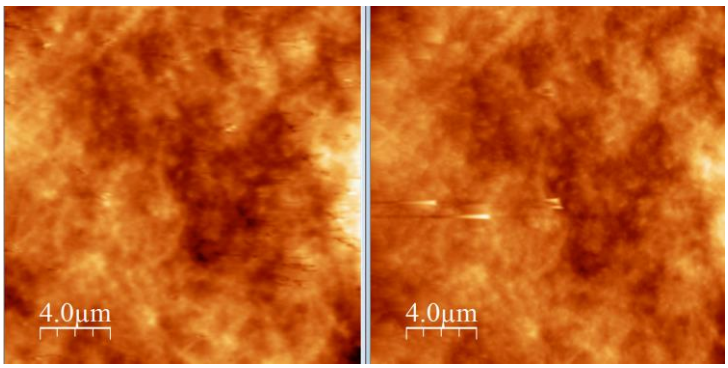

Figure 6: Contact and tapping mode images. The figures present the same exactly area of a collagen gel as it was imaged with contact and tapping mode respectively (the images were taken with a Cypher ES, Asylum, Oxford Instruments microscope with CSG10m NT-MDT probes).

3.3. Non - contact mode

In non - contact mode the applied force on the tip is attractive due to the fact that the tip is not in contact with the sample (Figure 7). The cantilever is oscillated near its resonance frequency under the influence of an alternating voltage due to a

piezoelectric element. During the relative motion of the sample's surface toward the tip, the oscillation amplitude is reduced and the oscillation frequency of the cantilever changes due to the interaction forces between tip – sample (i.e. dominant repulsive interactions lead to a decrease of the resonance frequency). However, during the imaging procedure the frequency change remain constant. The interaction forces between tip and sample are smaller than in contact mode. The non – contact mode applies in very soft samples (e.g biological samples) in order to avoid scratching the sample's surface. In addition, it must be noticed that the non – contact mode is mostly applied in high vacuum environment [26]. Despite the fact that the non contact mode can provide valuable results (Ohnesorge F. M. Surf. Interface Anal. 1999, 27, 379), it is not used in air due to the fact that the non contact conditions can be hardly maintained due to the presence of the surface contamination layer.

a)

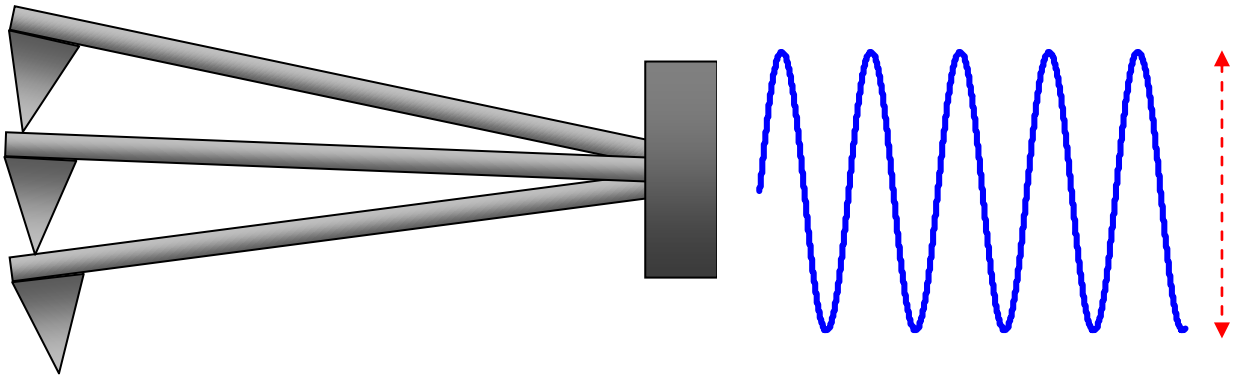

b)

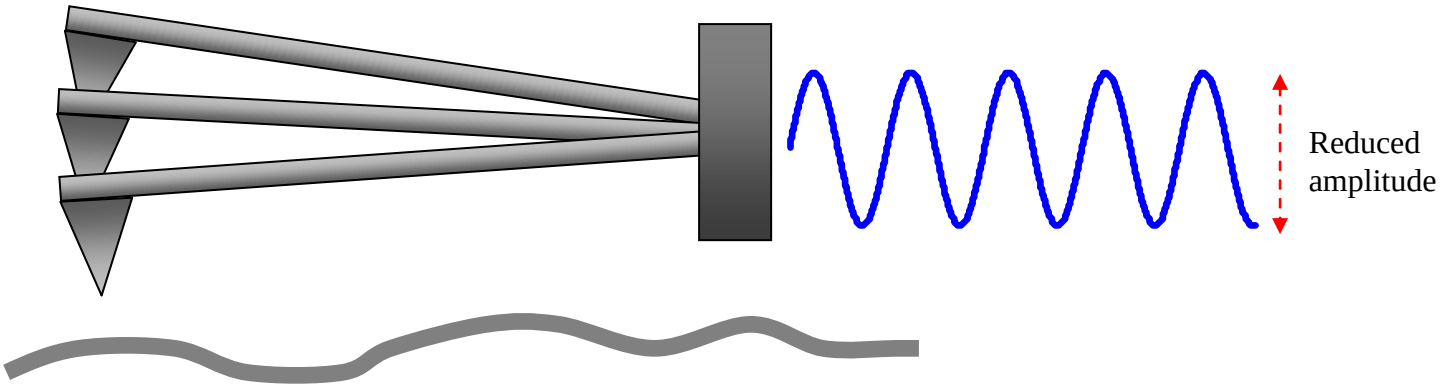

Figure 7: Non – contact mode. a) The cantilever is oscillated near its resonance frequency. b) During the relative motion of the sample's surface toward the tip, the oscillation amplitude is reduced and the oscillation frequency of the cantilever changes due to the interaction forces between tip – sample.

3.4. The applied forces in the AFM imaging modes

The choice of the AFM imaging mode is performed depending on the sample that must be tested. For non – biological sample, the contact mode can be used which is easily applied and there in no possibility of harming the sample. For very soft biological samples the non – contact mode is a reasonable choice. However, the low resolution imaging of non – contact mode leads to the application of tapping mode for biological samples. In contact mode the tip is always in contact with the sample's surface and the resultant force is repulsive. In non - contact mode, the tip is never in contact with the sample during the imaging procedure. Hence, the interaction force between tip – sample is attractive. In tapping mode, the tip is moving away and to the sample's surface, thus depending on the tip – sample distance the net force can be attractive or repulsive. In Figure 8, the net force in relation to distance is presented. In the diagram the blue box shows the interaction forces range in contact mode and the pink and green box the range of the interaction forces in the non – contact and the tapping mode respectively.

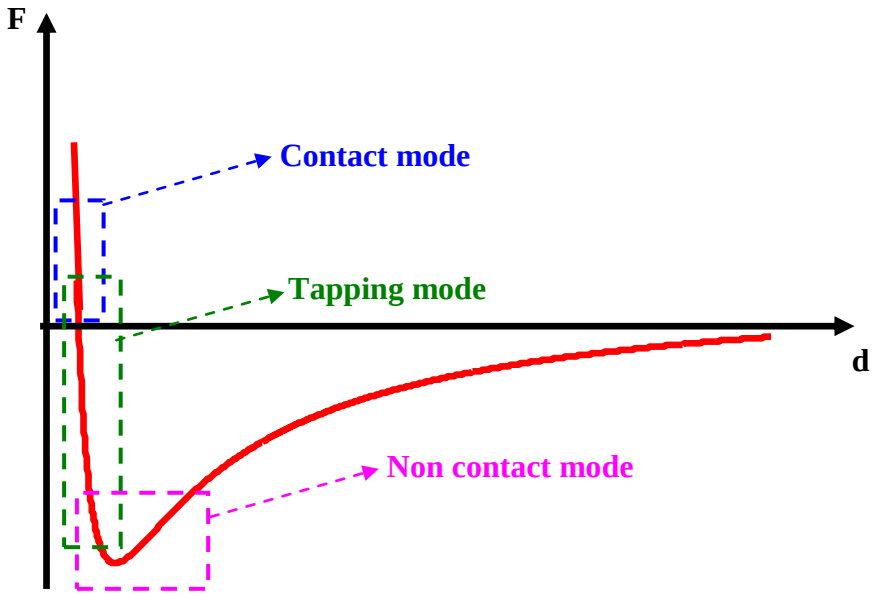

Figure 8: Force – distance diagram. In contact mode, the interaction force between the tip and the sample is repulsive. In non – contact mode the interaction force is attractive and in tapping mode, the interaction can be attractive or repulsive depending on the exact distance of the tip in relation to the sample's surface.

4. Force spectroscopy

4.1. The force – displacement curves

AFM provides the ability to determine the mechanical properties of a sample using the force spectroscopy [12, 14, 27]. The force spectroscopy is performed by moving the sample up and down towards the tip in order to measure the cantilever's

corresponding deflection. As a result a cantilever's deflection – displacement curve can be created at a single location of the tested sample's surface. The curve is created by measuring the bending of the cantilever during the up and down movement of the sample. The cantilever's deflection leads to the calculation of the applied force on the sample, using the simple equation $F=kd$, where F is the applied force, k the cantilever's spring constant and d the cantilever's deflection. The force displacement curve (Figure 9) has two curves, the loading curve (the sample's movement is towards the tip) and the unloading curve (the sample's movement is away from the tip).

The right side of the curve (in which F=0, the cantilever is undeflected) represents the area in which the AFM tip is far away from the sample's surface (i.e the scanner tube is fully retracted). As the sample is moving towards the sample, the tip 'jumps into' the sample due to a thin layer of humidity on the sample's surface which is responsible for a negative (attractive) net force on the tip (snap in point in Figure 9). The sample's motion towards the tip continues until the cantilever is bent away from the tip (repulsive net force) until the deflection reach the selected value (maximum applied force). After the fully extension of the scanner, it begins the opposite motion (i.e. to retract). The separation between the sample's surface and the tip occurs at the snap out point in which the net force is negative (the thin layer of humidity on the sample's surface applies a strong attractive force on the AFM tip). It must be noticed, that horizontal offset between the loading and the unloading curve is a result of scanner hysteresis. In addition, the shift between the loading and the unloading curve can also be the inverse of what is depicted in Figure 9. It must also be mentioned that the approach and retraction curves may also not coincide due to mechanical behaviours of the sample, i.e. plasticity, viscoelasticity, viscoplasticity e.t.c.
In addition, it must be noticed that the graph in Figure 9 represents a force – displacement curve obtained on a hard sample in which no indentation occurs. However, in many sample (e.g. the biological samples) the motion towards the tip (z) is larger that the cantilever's deflection (d), due to the indentation. The relation between the piezo – movement of the sample and the indentation (h) is $z = h + d$ (Figure 10). Hence the difference between the piezomovement of the sample and the cantilever's deflection is equal to the indentation depth.

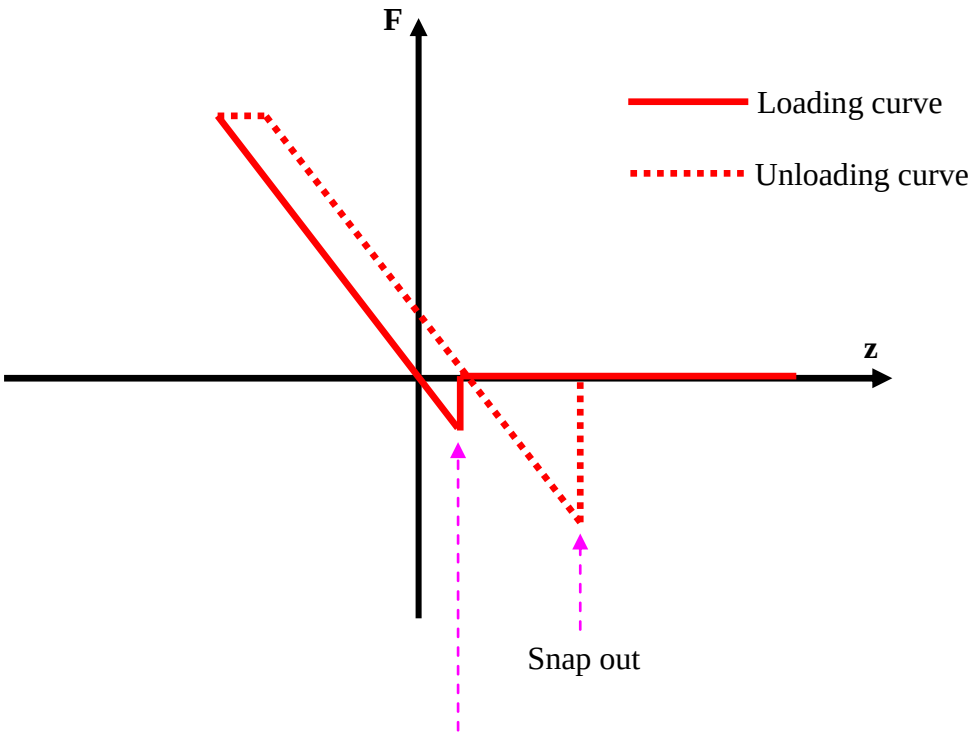

Snap in

Figure 9: A force – displacement curve obtained on a hard sample in air environment. The loading part of the curve represents the movement of the sample towards the tip. The unloading part represents the opposite movement of the sample (away from the tip). The snap in point represents the first contact of tip – sample's surface. The snap out point represents the point in which the tip separates from the sample.

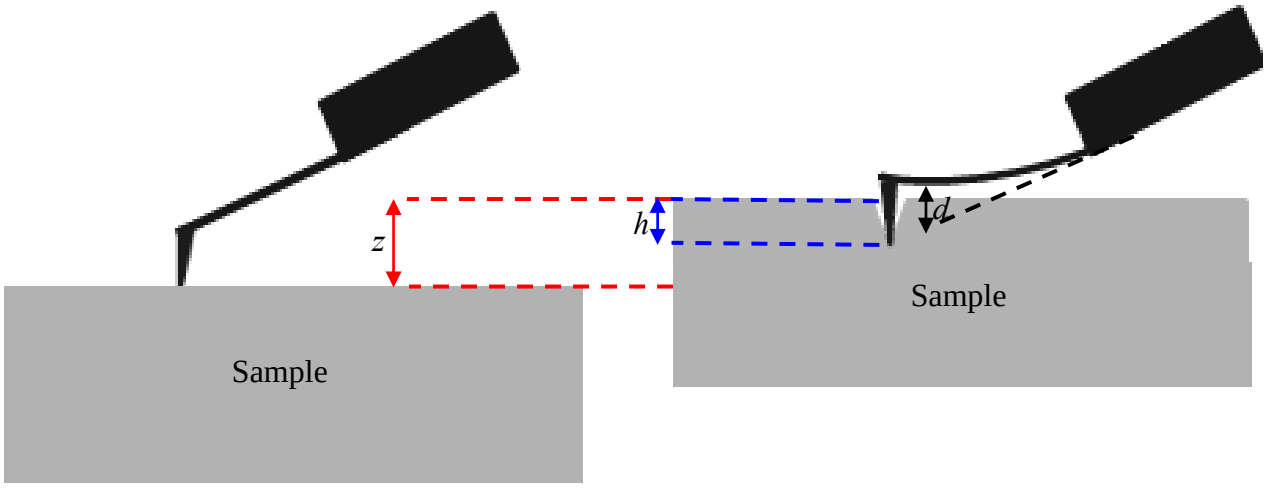

Figure 10: The sample's motion towards the AFM tip. The sample's movement (z) is equal to the sum of the cantilever's deflection (d) and the indentation into the sample (h).

In practice, in order to calculate the indentation depth for a specific applied force, a hard reference sample must be firstly used in which no indentation occurs. The reference sample must be several orders of magnitude stiffer that the tip, in order not to be intended. Using, a reference sample the piezo – movement is equal to the cantilever's deflection since the indentation depth is zero (h=0). In addition, the force – displacement curve on a stiff sample is linear (the applied force is proportional to the piezomovement of the sample, since z=d).

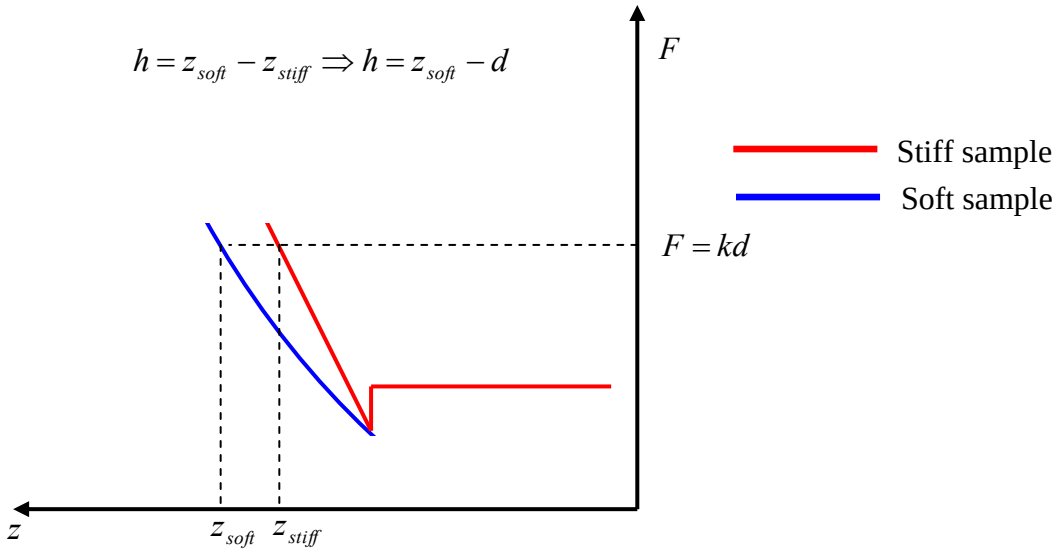

Figure 11: Unloading force – displacement curves for a stiff and a soft sample. The vertical axis represents the applied force on the sample's surface and the horizontal axis the piezomovement (motion of each sample).

After the acquisition of the linear curve on the hard reference sample, a force displacement curve must be obtained on the soft sample of interest. The indentation depth for every applied force value can be obtained by creating a force – indentation curve. The difference in the piezo - displacement for the hard and the soft sample in order to succeed the same cantilever's deflection results in the indentation depth (Figure 11) [12, 27]. The comparison of the force displacement curves on the soft and the stiff sample is generally carried out using the unloading curves [5, 6, 27]. Deformation during loading can probably be both elastic and plastic. However, during unloading, only the elastic displacements are recovered (the elastic nature of the unloading curve facilitates the analysis) [6].
A hard sample (AFM grating), a biological sample (collagen fibril) and the unloading force - displacement curves (obtained on the hard sample and on collagen, black and red curve respectively) are presented in Figure 12.

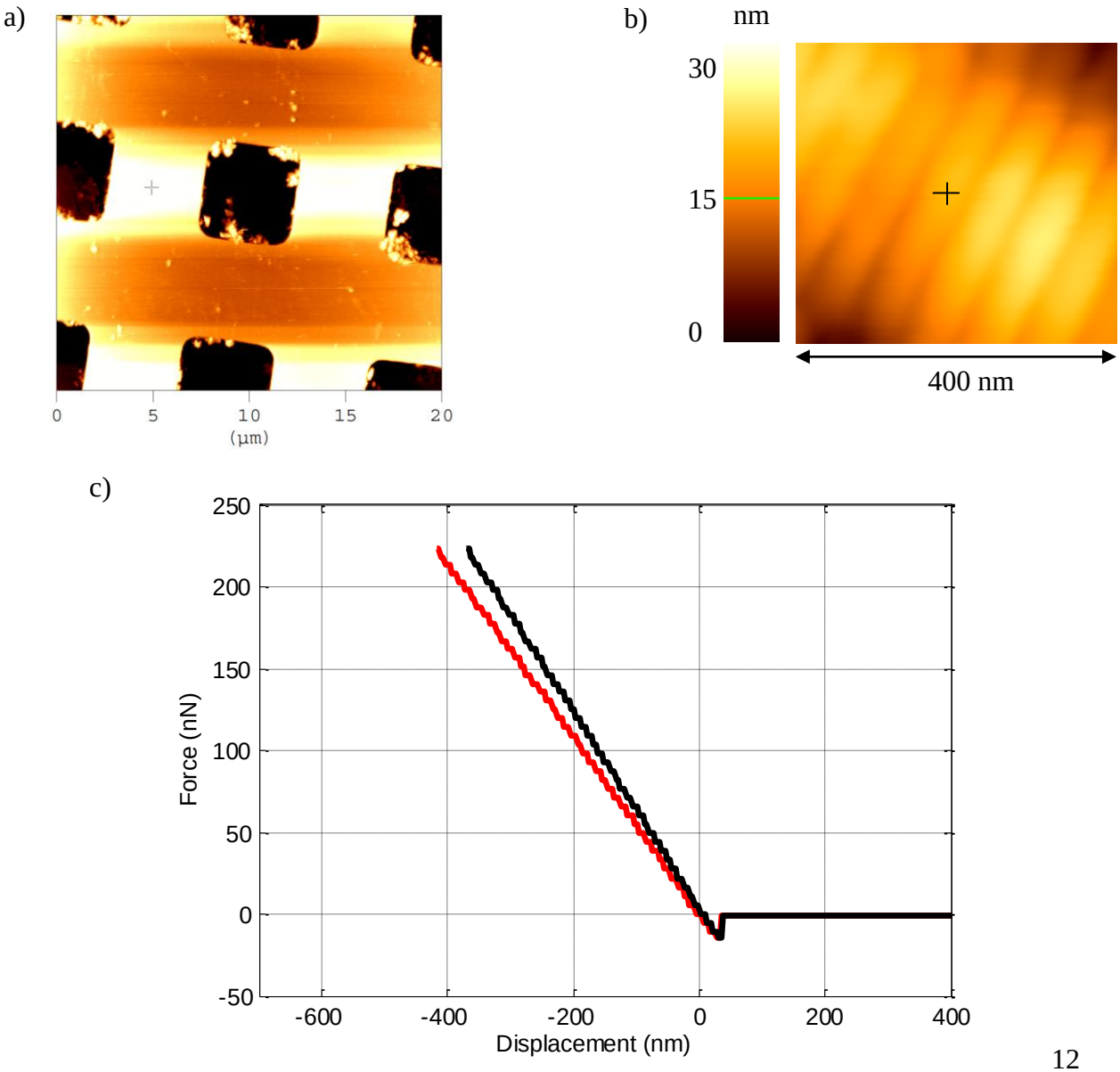

Figure 12: Unloading force – displacement curves for a stiff (AFM grating) and a biological sample (collagen). a) A hard sample reference (AFM grating). b) A biological sample (collagen fibril with radius ~350nm). c) Diagram of two force – displacement curves. The black curve was obtained on the hard reference sample (at the point of the cross, figure a) and the red curve was obtained on collagen fibril (at the point of the cross, figure b). (The image and the force displacement curves were obtained with a Veeco CPII atomic force microscope with MLCT (Bruker) type probes).

4.2. The application of the contact mechanism theory on AFM experiments

As it was presented in section 4.1 AFM tip can be used as an indenter in order to apply controlled vertical force to a sample's surface [4, 12, 27]. Depending on the tip's shape and the indentation depth, the AFM tip can be approximated as a solid sphere, cone or paraboloid of revolution [12, 28 - 29]. Hence, the classic theory of Hertz model can be approximately applied and provide valuable results. The Hertz model (which is the most widely applied model) was firstly established to describe the contact of two spherical elastic bodies. However, several extensions were made in order to include other basic indenter's geometries [30]. The most basic extension is the consideration of the sample as an elastic half space. In addition, in case of a rigid cone, indenting a soft flat surface (elastic half space), the Sneddon model can be applied. In the most AFM experiments, the AFM tip radius is several orders of magnitude smaller than the dimensions of the sample. Hence, the interaction between the tip and the sample can be considered as the interaction between and indenter and an elastic half space.
In addition, the application of the Hertz model is valid under the following assumptions [31]:

1. The sample is isotropic and homogeneous.
2. The contact between tip – sample is adhesionless and frictionless.
3. The contact geometry is assumed to be axisymmetric, smooth and continuous.

4.2.1. The assumption of AFM tip as a sphere

Spherical AFM tips (Figure 13), like borosilicate glass spheres can be used for an indentation experiment, mostly on biological samples (e.g. cells, articular cartilage) [28]. In addition, if the AFM tip has a pyramidal geometry but the indentation depth is small comparing to the tip radius, the AFM tip can be approximated as a sphere [27, 29].

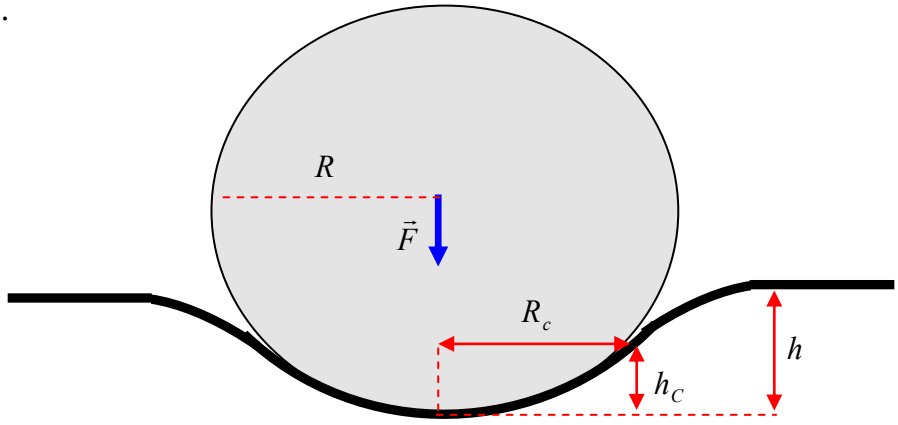

Figure 13: Assumption of an AFM tip as a sphere with radius R. In the above illustration, F is the applied force, h the indentation depth and Rc the radius at the contact depth hc.

The relationship between the applied force and the indentation depth is provided by the equation [8]:

$$F = \frac{4}{3} E^* R^{1/2} h^{3/2} \tag{2}$$

where, F is the applied force, E^* is the combined elastic modulus of the contacting bodies, R is the tip radius and h the indentation depth. In addition,

$$\frac{1}{E^*} = \frac{1-\nu^2}{E} + \frac{1-\nu_i^2}{E_i} \tag{3}$$

where, E_i and ν_i, and E and ν, represent the elastic modulus and Poisson ratio of the indenter and the specimen, respectively.
However, providing that the tip is several orders of magnitude stiffer than the sample, equation (3) can be expressed in the form:

$$\frac{1}{E^*} = \frac{1-\nu^2}{E} \tag{4}$$

Hence, equation (2) is transformed as follows:

$$F = \frac{4ER^{1/2}h^{3/2}}{3\left(1-\nu^2\right)} \tag{5}$$

The Young's modulus can be easily calculated using the linearized Hertz model [8, 32-33]. The slope S of the linear curve $F^{2/3} - h$ leads to the calculation of the Young's modulus value (Figure 14). The linearized force indentation curves are expressed by the equation:

$$F^{2/3} = \left[\frac{4ER^{1/2}}{3\left(1-\nu^2\right)}\right]^{2/3} h \Rightarrow F^{2/3} = Sh \tag{6}$$

where $S = \left[\frac{4ER^{1/2}}{3\left(1-\nu^2\right)}\right]^{2/3}$ is the slope of the linear curve $F^{2/3} - h$. In conclusion, the Young's modulus is calculated by the equation:

$$E = \left[\frac{3\left(1-\nu^2\right)}{4R^{1/2}}\right] S^{3/2} \tag{7}$$

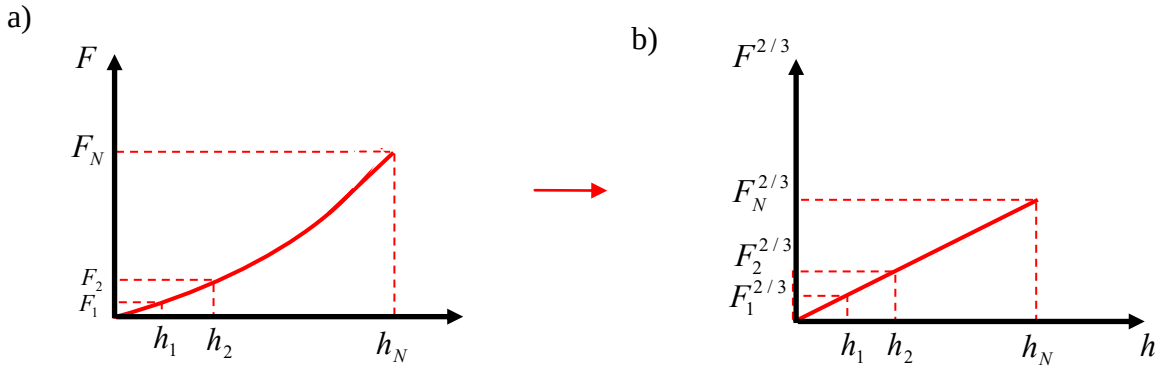

h

Figure 14: Force – indentation curves. a) Force – indentation curve on a single point. b) Force curve of the linearized Hertz model.

Similar analysis can be done, in the case of considering the tip as a paraboloid of revolution (Figure 15). If the indentation depth is much smaller than the tip radius the Young's modulus can be calculated using the same equations [27, 29, 34].

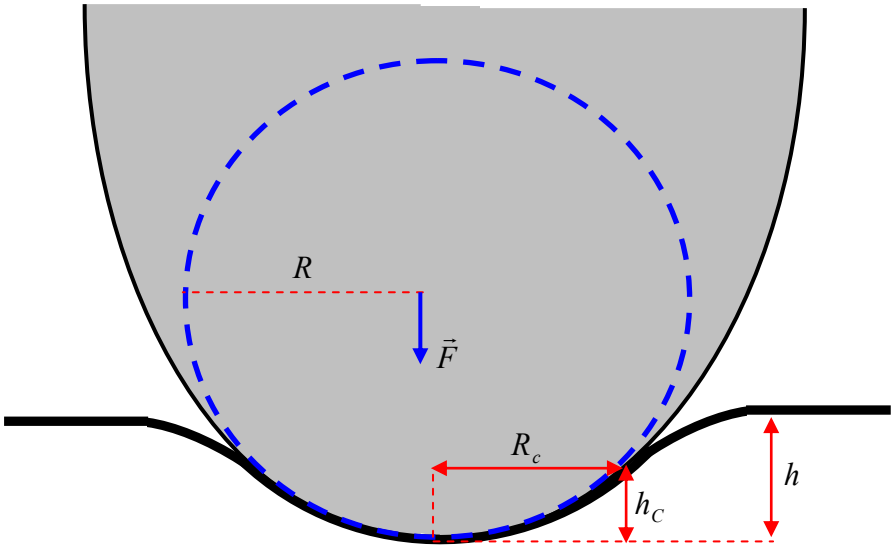

Figure 15: **Assumption of a hard pyramidal AFM tip as a paraboloid of revolution.** In the case of small indentation depths (h<R) it can be approximated by a sphere.

4.2.2. The assumption of AFM tip as a cone (Sneddon model)

Most of the tips which are used in AFM experiments have pyramidal geometry. If the indentation depth is high the pyramidal tip can be approximated to a cone (Figure 16) which results in the same projected area to the pyramidal tip.
The relationship between the applied force and the indentation depth (in case that the tip is several orders of magnitude stiffer than the sample) is provided by the equation [35-36]:

$$F = \frac{2E(\tan\theta)h^2}{\pi(1-\nu^2)} \tag{8}$$

where, F is the applied force, E, ν are the elastic modulus and the Poisson's ratio of the sample respectively, θ is the cone half - angle h the indentation depth. Using the equation (8) the Young's modulus of the sample can be easily determined.

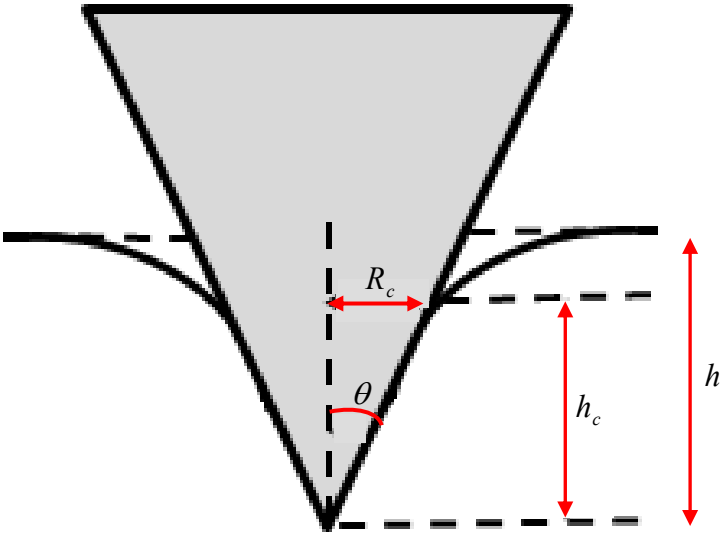

Figure 16: **Assumption of a hard pyramidal AFM tip as a cone.**

4.2.3. The calculation of the Young's modulus using general equation

The Young's modulus can be also calculated using the basic formula [5-6, 12, 27, 31]:

$$E = \frac{\sqrt{\pi}}{2}\left(1-\nu^2\right)\frac{S}{\sqrt{A_c}} \tag{9}$$

where, E is the Young's modulus, ν the sample's Poisson's ratio, S the contact stiffness, and A_c an area function related to the effective cross-sectional or projecting area of the indenter. The contact stiffness can be determined by the slope of the upper unloading part of the force – indentation curve, thus $S = \left.\frac{dF}{dh}\right|_{h_{\max}}$ [5, 6, 12, 27, 31]. Equation (9) can be applied in every case of a rigid smooth frictionless axisymmetric indenter [31] (regardless the indenter's shape). However, it must be noticed that the projecting area depends on the tip's shape.
For spherical indenters [29]:

$$A_c = \pi h_c^2\left(2R - h_c\right) \tag{10}$$

For conical indenters [37]:

$$A_c = \pi h_c^2 \tan^2\theta \tag{11}$$

The depth at which contact is made between indenter and the sample during indentation is defined as contact depth h_c [5, 6, 12, 27, 31].

$$h_c = h_{\max} - \varepsilon\frac{P_{\max}}{S} \tag{12}$$

,where h_{max} is the maximum indentation depth and ε is a constant that depends on the indenter geometry. For conical geometry ε = 0.72 and for paraboloid of revolution geometry ε=0.75 [31]. Contact depth is illustrated in Figures 13, 15,16.
In addition, it must be noticed that he typical Poisson's ratio v of a solid material is in the range of $0 < v < 0.5$. However, the uncertainty of exact value of the Poisson's ratio provides uncertainty in the Young's modulus calculation. Hence, in order to avoid the uncertainty of the exact value of Poisson's ratio, the reduced modulus, $E^* = \frac{E}{1-v^2}$ can be calculated.

5. Young's modulus maps

5.1. Force Volume Mode

Force spectroscopy can also be extended in the so called Force Volume Mode. In this mode the force – displacement curves are obtained from a large number of points of the region of interest. After acquiring the force-distance curves the Young's modulus for each point can be calculated and the Young's modulus values for every point can be presented in a Young's modulus map (Figure 17) [38].

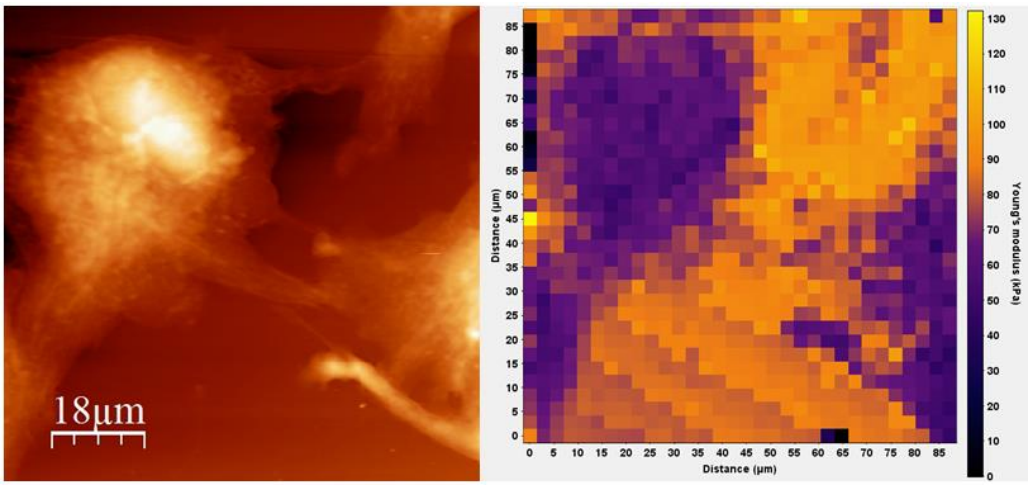

Figure 17: **Topography and Young's modulus map of cancer associated fibroblasts**. The images were acquired with a PicoPlus, Molecular Imaging/Agilent microscope, in contact mode under PBS with SICON, Applied NanoStructures. The data processing was accomplished by the open source software called AtomicJ An open source software for analysis of force curves [39].

5.2. Force Scanning Method

A Young's modulus map can be alternatively created using the force scanning method [8, 32-33]. In the force scanning method, a specific area is being scanned several times with different set point forces. Each obtained image is characterized by z-values (which represent the height of each point). The indentation values are calculated by subtracting the z – values from an arbitrary contact-point height z_0 [8]. Hence, the creation of arrays which consist of indentation values at every point of the scanned

area leads to the calculation of the Young's modulus values at each point of the image (i.e. the creation of the Young's modulus map]. The Young's modulus value for each point is calculated using the linearized Hertz model as it was presented in section 4.2.1.

6. Advanced Techniques

6.1. Peak Force Tapping mode

The operation of the Peak Force Tapping mode is similar to the tapping mode due to the fact that the lateral forces are avoided by intermittently contact with the sample. However, it must be noticed that its operation is in a non-resonant mode. Its major advantage is that it combines the benefits of tapping and contact mode imaging (i.e. direct force control and avoidance of lateral forces) (Kaemmeret al.). The oscillation in the Peak Force Tapping mode is performed at all frequencies well below the cantilever resonance. A typical frequency for the probe oscillation is 2 kHz (which is far below the resonant frequency of the cantilever). Typical peak to peak amplitudes in air are ~300nm[Derjaguin et al.]. The probe is periodically onto contact with the sample's surface for a short time period (<100μs) [Derjaguin et al.]. Hence, a periodically force is applied onto the sample's surface. Thus, individual force – seperation curves can be created and collected for each 'tap' of the tip onto the sample's surface. The innovation of the Peak Force Tapping mode is based on the control of the peak force (maximum normal force) which is applied on the sample's surface at each point. Using the feedback system, the maximum applied force is kept constant during scanning. The data about adhesion forces, surface deformation and topography are separated from the individual force – seperation curves at each position. The principles of the force – separation curves are comparable to the force – displacement curves for the Young's modulus calculation in the classic nanoindentation procedure. For the estimation of the mechanical properties of the sample using the Peak Force Tapping mode, the Derjaguin–Muller–Toporov (DMT) model [Derjaguin et al.] can be used, which leads to the estimation of the sample's reduced modulus which is described by the following equation:

$$F_{INT} = \frac{4}{3} E^* \sqrt{R(d - d_0)^3} + F_{ADH}$$

Where F_{INT} is the tip –sample force, E^* is the combined reduced modulus (of the tip and the sample), R is the tip radius, d_0 is the rest position of the surface, $d - d_0$ the sample's deformation and F_{ADH} the adhesion force during contact.

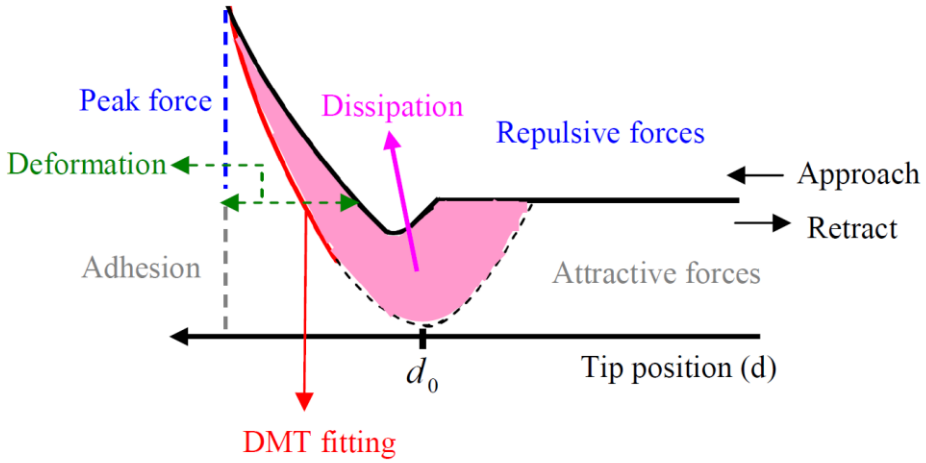

Figure 18: **Force – separation curve.** Illustration of a force – separation curve using the Peak Force Tapping mode (Pittenger et al.). The maximum force is constant for each measurement.

6. Force spectroscopy in biological samples and biomaterials

Atomic Force Microscopy has been extensively used for the mechanical characterization of biomaterials in nanoscale. The determination of the Young's modulus of biomaterials and biological samples like collagen, cells or articular cartilage under various conditions is of great importance for Biophysics research. Hence, typical results from the literature are provided in the next sections. In addition, typical Young's modulus values of collagen, cells and articular cartilage under various conditions are presented in Table 1.

6.1. Collagen

The importance of collagen in Biophysics and Biomaterials research is high due to its big amount in mammals. Specifically, most parts of the mammalian body, (e.g., tissue, skin, bone, cartilage, or tendons) contain collagen in the form of collagen fibrils. Hence, the mechanical characterization of collagen in nanoscale is crucial. Many researchers have calculated Young's modulus of collagen fibrils. In particular, M.M Jolandan et al. [40] investigated the mechanical heterogeneity of the collagen fibrils type I due to the D-band periodicity. The resulted average values were ~2.2 GPa and ~1.2 GPa for the overlapping and the gap regions, respectively. Furthermore, the resulted alteration of the Young's modulus values between gap and overlapping regions was confirmed by Kontomaris et al. [27] who estimated the Young's modulus of overlapping and gap regions of collagen fibrils type I in the range of 0.74 – 1.43GPa due to the mechanical heterogeneity of collagen fibrils. Moreover, Strasser et al [13] calculated the Young's modulus average values, of collagen fibrils type I, approximately 1.2 ± 1 GPa, while V.S. Yadavalli et al. estimated the Young's

modulus 1.03 ± 0.31 GPa [41]. Furthermore, the mechanical properties of collagen fibrils have been studied by A.J. Heim et. al, giving average values 1–2 GPa [14] and M.P.E. Wenger et al. whose results were in a range from 5 GPa to 11.5 GPa [29]. Due to the big stiffness of collagen (small indentation depths) the most common approximation of the tip for the Young's modulus calculation is the spherical approximation.

6.2. Cells

The determination of the mechanical properties of various types of cells is a critical issue in the scientific area of Biophysics. Many researchers have calculated Young's modulus of various types of cells. In particular, Mathur et al. determined the Young's modulus variations of human umbilical vein endothelial cells in the range 1 - 7 kPa. Murakoshi et al. calculated the Young's modulus of outer hair cells from the cochlea of mice equal to ~2kPa. Furthermore, the age-dependent apparent elastic modulus of cardiac myocytes was estimated by Lieber et al. in the range of 35 kPa to 43 kPa. Moreover, the values of human aortic endothelial cells were calculated equal to ~1.5 kPa and ~5.6 kPa for two distinct populations (Costa et al).

In addition, the determination of the cells' mechanical properties under various conditions is a crucial issue due to the fact that leads to the detection of pathological situations like cancer. In particular a change in cell Young's modulus is a characteristic of cancer cells [42]. The Young's modulus alteration has major importance due to the fact that affects the way that they spread [43]. Using AFM is possible for the scientists to calculate the Young's modulus of metastatic cancer cells from patients with suspected breast, lung and pancreas cancer [43, 44]. In particular, the cell stiffness of cancer cells can be ~70% softer compared with the benign cells (e.g., the Young's modulus of cancer cells obtained from a woman detected with breast ductal adenocarcinoma is in the range 0.50 ± 0.08 kPa. In contrast to the above result the Young's modulus of the normal cells was calculated in the range 1.93 ± 0.50 kPa) [43]. Hence, the mechanical analysis can distinguish normal from cancerous cells, even in cases that the normal and the cancerous cells have similar shapes.

Moreover, Efremov et al. studied the mechanical properties of cells with different levels of cancer transformation [45]. The transformed cells were found to be 40%-80% softer compared to the normal cells.

In addition Li et al. investigated the Young's modulus differences of breast epithelial cells and malignant breast epithelial cells using AFM. The Young's modulus of cancer cells was found significantly lower (1.4-1.8 times) compared to the normal epithelial cells at physiciological temperature ($37^{\circ}C$) [46].

The most common approximation of the tip for the Young's modulus calculation for cells is the spherical approximation, however the conical approximation can be also used [43, 45].

6.3. Articular Cartilage

The Young's modulus of articular cartilage can be also calculated using AFM. For example, it has been reported that the elastic modulus of the intercellular matrix of articular cartilage exhibits a depth-dependent increase from the articular surface (superficial zone: ~0.52 MPa, calcifying deep zone: ~1.69 MPa) (Patel et al. 2003, Tomkoria et al. 2004). In addition, Atomic Force Microscopy is a powerful tool which can provide information regarding the functionality of articular cartilage and detect diseases such as osteoarthritis at initial stages. The investigation of the mechanical properties of articular cartilage as a method of diagnosis of diseases at early stages has been reported by many researchers [28, 37, 47]. The results of Stolz et al. [28] who calculated the Young's modulus of normal articular cartilage in micro and nanoscale were 2.6 MPa and 0.021 MPa, respectively. In the same order of magnitude were the results by Loparic et al. who calculated the microstiffness of articular cartilage equal to 1.3 ± 0.4 MPa and the nanostiffness 22.3 ± 1.5 kPa (cartilage's soft proteoglycan (PG) gel) and 184 ± 50kPa (Collagen meshwork) [37]. In addition, Stolz et al. proved that in the early stages of osteoarthritis the microstiffness of articular cartilage remains constant. However, the early stages of osteoarthritis could be only detected at nanometer scale. According to Stolz research, the nanostiffness reduces from 83kPa (normal cartilage) to 5.6kPa (grade 3 of osteoarthritis) [47]. Hence, the ability to detect early changes on the cartilage mechanical properties, using AFM in nanometer scale has opened a new prospect of using atomic force microscopy even as a clinical tool.

Conclusion

In this paper, an overall review of the basic operation and applications of Atomic Force Microscopy on biomaterials was presented. The physical principles of nanoscale interactions between the AFM tip and the sample's surface were clearly explained. In addition, the ability of AFM for the mechanical characterization of a sample's surface was presented. The above paper will contribute to the literature as a tool for a coherent presentation of AFM basic operation and application regarding Biophysics and Nanotechnology students.

Acknowledgments

Research leading to these results has received funding from the Horizon 2020—Marie Skłodowska-Curie Individual Fellowship MSCA-IF-2014-658769 MYO-DESMOPLASIA (to AS).

Examples of AFM Measurements (Young's modulus)					
Collagen		**Cells**		**Articular Cartilage**	
Reference	Young's modulus	Reference	Young's modulus	Reference	Young's modulus
Kontomaris et al. (2015)	0.74 – 1.43GPa	Mathur et al. (2000)	Human umbilical vein endothelial cells (HUVECs) with regional variations $1-7$ kPa	Loparic et al. (2010)	Microscale 1.3 ± 0.4 MPa
Strasser et al. (2007)	1.2 ± 1 GPa	Murakoshi et al. (2006)	Outer hair cells from the cochlea of mice 2 kPa		Nanoscale 22.3 ± 1.5 kPa (PG) 184 ± 50kPa (Collagen)
Yadavalli et al. (2010)	1.03 ± 0.31 GPa	Lieber et al. (2004)	The age-dependent apparent elastic moduli of cardiac myocytes were in the range of 35 kPa to 43 kPa	Stolz et al. (2009)	Microscale 2.3 ± 0.4 Mpa Nanoscale 83 - 5.6kPa (depending of the stage of osteoarthritis)
Wenger et al. (2007)	3.75-11.5 GPa	Costa et al. (2006)	The values of human aortic endothelial cells were ~1.5 kPa and ~5.6 kPa for two distinct populations	Patel et al. 2003 Tomkoria et al. 2004	intercellular matrix of articular cartilage superficial zone: ~0.52 MPa, calcifying deep zone: ~1.69 MPa).
		Cross et al. (2007)	Normal cells 1.93 ± 0.50 kPa Breast ductal adenocarcinoma 0.50 ± 0.08 kPa		
Jolandan and Yu (2009)	~ 1.2 - 2.2 GPa	Li at al. (2008)	Young's modulus of cancer cells was found significantly lower (1.4-1.8 times) compared to the normal epithelial cells	Stolz et al. (2004)	Nanoscale 0.021 MPa
		Efremov et al. (2014)	Young's modulus of fibroblasts with different levels of cancer transformation were found to be 40-80% softer compared to normal fibroblasts		Microscale 2.6 MPa

Table 1: Typical measurements of Young's modulus on collagen, cells and articular cartilage using Atomic Force Microscopy.

References

[1] Binnig G, Quate C F and Gerber C 1986 Atomic force microscope Phys. Rev. Lett. 56 930–3

[2] Alessandrini A and Facci R 2005 AFM: a versatile tool in biophysics Meas. Sci. Technol. 16 R65–R92

[3] Allison D P, Mortensen N P, Sullivan C J, Doktyczl M J 2010 Atomic force microscopy of biological samples Wiley Interdiscip. Rev. Nanomed. Nanobiotechnol. 2 618-34

[4] Mateu M G 2012 Mechanical properties of viruses analyzed by atomic force microscopy: A virological perspective Virus Research 168 1– 22

[5] Oliver W C, Pharr G M 1992 An improved technique for determining hardness and elastic modulus using load and displacement sensing indentation experiments J Matter Res vol. 7 1564-1583

[6] Oliver W C, Pharr G M 2004 Measurement of hardness and elastic modulus by instrumented indentation: Advances in understanding and refinements to methodology J Mater Res 19 3-20

[7] Feng Z Q, He Q C, Zeng Q, Joli P 2010 Handbook of Nanophysics Taylor & Francis 26, 26-1 – 26-15

[8] Darling E M 2011 Force scanning: A rapid, high-resolution approach for spatial mechanical property mapping. Nanotechnology 22, 175707

[9] Kurland N E, Drira Z, Yadavalli V K 2012 Measurement of nanomechanical properties of biomolecules using atomic force microscopy Micron 43 116–128

[10] Stylianou A, Kontomaris S V and Yova D 2014 Assessing Collagen Nanoscale Thin Films Heterogeneity by AFM Multimode Imaging and Nanoindetation for NanoBioMedical Applications Micro and Nanosystems 6 95-102

[11] Stylianou A, Yova D and Alexandratou E 2014 Investigation of the influence of UV irradiation on collagen thin films by AFM imaging Mat Sci Eng C 45 455-468

[12] Kontomaris SV, Yova D, Stylianou A and Politopoulos K 2015 The significance of the percentage differences of Young's modulus in the AFM nanoindentation procedure Micro and Nanosystems 7 86-97

[13] Strasser S, Zink A, Janko M et al. 2007 Structural investigations on native collagen type I fibrils using AFM Biochem Bioph Res Co 354 27-32

[14] Heim A J, Matthews W G and Koob T J 2006 Determination of the elastic modulus of native collagen fibrils via radial indentation Appl Phys Lett 89

[15] Jalili N, Laxminarayana K 2004 A review of atomic force microscopy imaging systems: application to molecular metrology and biological sciences Mechatronics 14 907–945

[16] Planinsic G, Lindell A, Remskar M 2009 Themes of nanoscience for the introductory physics course Eur. J. Phys. 30 S17–S31

[17] Morris V J, Kirby A R, Gunning A P 2008 Atomic Force Microscopy for Biologists. Atomic Force Microscopy for Biologists, vol Book, Whole. Imperial College Press, London

[18] Kuznetsov Y G, McPherson A 2011 Atomic force microscopy in imaging of viruses and virus-infected cells Microbiol. Mol. Biol. Rev 75 268-285

[19] Bergmann A, Feigl D, Kuhn D, Schaupp M, Quast G, Busch K, Eichner L and Schumacher J 2013 Low-cost AFM setup with an interferometer for undergraduates and secondary-school students Eur. J. Phys. 34 901–914

[20] Seo Y and Jhe W 2008 Atomic force microscopy and spectroscopy Rep. Prog. Phys. 71 016101

[21] Kasas S, Thomson N H, Smith B L, Hansma P K, Miklossy J, Hansma H G 1997 Biological Applications of the AFM: From Single Molecules to Organs, Int. J. Imag. Syst. Tech. 8 151–161.

[22] García R and Pérez R 2002 Dynamic atomic force microscopy methods Surface Science Reports 47 197-301.

[23] Putman C A, van der Werf K O, de Grooth B G, van Hulst N F, Greve J and Hansma P K 1992 A new imaging mode in atomic force microscopy based on error signal SPIE Scanning Probe Microsc. 1693 198–204.

[24] Asylum Research, an Oxford Instrument company “Application Guide”, version 13, revision A-1714, dated 10/25/2013

[25] Habelitz S, Balooch M, Marshall SJ, Balooch G, Marshall Jr GW 2002 In situ atomic force microscopy of partially demineralized human dentin collagen fibrils. Journal of Structural Biology 138 227-36

[26] Majid M J 2010 Scanning Probe Microscopy of Biomaterials and Nanoscale Biomechanics Dissertation, University of Illinois at Urbana-Champaign, 2010

[27] Kontomaris SV, Stylianou A, Yova D and Balogiannis G. 2015 The effects of UV irradiation on collagen D – band revealed by atomic force microscopy Scanning 37 101-11

[28] Stolz M, Raiteri R, Daniels A U, Van Landingham M R, Baschong W, Aebi U 2004 Dynamic Elastic Modulus of Porcine Articular Cartilage Determined at Two Different Levels of Tissue Organization by Indentation-Type Atomic Force Microscopy Biophys J 86 3269-83
[29] Wenger MPE, Bozec L, Horton MA and Mesquidaz P 2007 Mechanical properties of collagen fibrils. Biophys J 93 1255-63

[30] Johnson K L Contact mechanics 1985 Cambridge University Press.

[31] Fischer-Cripps A C 2007 Introduction to contact mechanics, Second ed. New York: Springer.

[32] Kontomaris S V, Yova D, Sambani K, Stylianou A 2016 AFM Investigation of the Influence of Red Light Irradiation on Collagen IFMBE proceedings 57 269-74

[33] Stylianou A, Kontomaris S V, Yova D 2016 Probing Collagen Nanocharacteristics after Low-Level Red Laser Irradiation IFMBE proceedings 57 264-8

[34] Kontomaris S V, Stylianou A, Yova D, Politopoulos K 2012 Mechanical Properties of Collagen Fibrils on Thin Films by Atomic Force Microscopy Nanoindentation BIBE Proccedings 608-13

[35] Kuznetsova T G, Starodubtseva M N, Yegorenkov N I, Chizhik S A, Zhdanov R I 2007 Atomic force microscopy probing of cell elasticity Micron 38 824–33

[36] Laurent V M, Kasas, S, Yersin A., Schaffer T E, Catsicas S, Dietler G, Verkhovsky A B, Jean-Jacques Meister J J 2005 Gradient of rigidity in the lamellipodia of migrating cells revealed by atomic force microscopy Biophys. J. 89 667–75.

[37] Loparic M, Wirz D, Daniels AU, Raiteri R, VanLandingham M R , Guez G, Martin I, Aebi U, Stolz M 2010 Micro – and Nanomechanical analysis of Articular Cartilage by Indentation – type Atomic Force Microscopy: Validation with a Gel Microfiber Composite Biophys J 98 2731–40.

[38] Han W S, Force Spectroscopy with the Atomic Force Microscope-Application Note. Agilent Technologies.http://cp.literature.agilent.com/litweb/pdf/5989-8215EN.pdf

[39] Hermanowicz P, Sarna M, Burda K, Gabryś H 2014 AtomicJ: An open source software for analysis of force curves. Review of Scientific Instruments 85 063703.

[40] Minary-Jolandan M, Yu M 2009 Nanomechanical heterogeneity in the gap and overlap regions of type I collagen fibrils with implications for bone heterogeneity Biomacromolecules 10: 2565-70

[41] Yadavalli V K, Svintradze D V, Pidaparti R M 2010. Nanoscale measurements of the assembly of collagen to fibrils. Int. J. Biol. Macromol. 46: 458-64

Stefan B. Kaemmer 2011 Introduction to Bruker's ScanAsyst and PeakForce Tapping AFM Technology Corporation Application Note 133, www.bruker-nano.com.

B.V. Derjaguin, V.M. Muller, Y.P. Toporov, Effect of contact deformations on adhesion of particles, J. Colloid Interface Sci. 53 (1975) 314.

B. Pittenger, N. Erina, C. Su, Quantitative Mechanical Property Mapping at the Nanoscale with PeakForce QNM, Bruker Corporation Application Note AN128, www.bruker-nano.com2010.

[42] Gretsi V, Stylianou A, Papageorgios P, Polydorou C and Stylianopoulos T 2015. Remodeling components of the tumor microenvironment to enhance cancer therapy Front. Oncol. 5 (214),

[43] Cross S E, Jin Y S, Rao J, Gimzewski J K 2007 Nanomechanical analysis of cells from cancer patients Nat. nanotechnol. 2 780-3

[44] Stylianou A and Stylianopoulos T 2016. Atomic Force Microscopy Probing of Cancer Cells and Tumor Microenvironment Components BioNanoScience 6 33-46.

[45] Efremov Y M, Lomakina M E, Bagrov D V Makhnovskiy, Alexandrova A Y, Kirpichnikov M P, Shaitan K V 2014 Mechanical properties of fibroblasts depend on level of cancer transformation Biochim. Biophys. Acta 1843 1013–19

[46] Li Q S, Lee G Y H, Ong C N, Lim C T 2008 AFM indentation study of breast cancer cells Biochem. Biophys. Res. Commun. 374 609–13

[47] Stolz M, Gottardi R, Raiteri R, Miot S, Martin I, Imer R, Staufer U, Raducanu A, Düggelin M, Baschong W, Daniels AU, Friederich NF, Aszodi A, Aebi U. 2009. Early detection of aging cartilage and osteoarthritis in mice and patient samples using atomic force microscopy Nat. Nanotechnol. 4 186-92.